A Structural Neural System for Real-time Health Monitoring of Composite Materials

Goutham R. Kirikera, Vishal Shinde, Mark J. Schulz, Anindya Ghoshal, Mannur J. Sundaresan, Randall J. Allemang and Jong Won Lee

Structural Health Monitoring 2008 7: 65
DOI: 10.1177/1475921707081971

SHM
Structural Health Monitoring

A Structural Neural System for Real-time Health Monitoring of Composite Materials

Goutham R. Kirikera,[1,†,*] Vishal Shinde,[2,†] Mark J. Schulz,[3] Anindya Ghoshal,[4] Mannur J. Sundaresan,[5] Randall J. Allemang[6] and Jong Won Lee[7,†]

[1]*Center for Quality Engineering and Failure Prevention, Department of Mechanical Engineering, CAT Building, RM 327, 2137 N.Sheridan Road, Evanston, IL 60208*
[2]*195 Clarksville Rd, Physical Acoustics Corporation, Princeton Jn, NewJersey, 08550*
[3]*Smart Structures Bio-Nanotechnology Laboratory (SSBNL), 408B Rhodes Hall Department of Mechanical Engineering, University of Cincinnati, Cincinnati, OH USA, 45221*
[4]*United Technology Research Center, 411, Silver Lane, MS 129-73 East Hartford, CT 06108, USA*
[5]*Intelligent Structures and Mechanisms Laboratory, Department of Mechanical Engineering, North Carolina A&T state University, Greensboro, NC 27411, USA*
[6]*Structrual Dynamics Research Laboratory, 593 Rhodes Hall, Department of Mechanical Engineering, University of Cincinnati, Cincinnati, OH, 45221*
[7]*Korea Institute of Machinery and Materials, Daejeon, Korea*

A prototype structural neural system (SNS) is tested for the first time and damage detection results are presented in this study. The SNS is a passive online structural health monitoring (SHM) system that mimics the synaptic parallel computation networks present in the human biological neural system. Piezoelectric ceramic sensors and analog electronics are used to form neurons that measure strain waves generated by damage. The sensing of strain waves is similar to the proven nondestructive evaluation (NDE) technique of acoustic emission (AE) monitoring. Fatigue testing of a composite specimen on a four-point bending fixture is performed, and the SNS is used to monitor the specimen for damage in real time. The prototype SNS used four sensors as inputs, but the number of inputs can be in the tens or hundreds depending on the type of SNS processor used. This is an area of continuing development. The SNS has two channels of signal output that are digitized and processed in a computer. The first output channel tracks the propagation of waves due to damage, and the second output channel provides the combined AE responses of the sensors. The data from these two channels are used to predict the location of damage and to qualitatively indicate the severity of the damage. Overall, this study shows that the SNS can detect damage growth in composites during operation of the structure, and the SNS architecture has the potential to tremendously simplify the AE technique for use in on-board SHM. Ten or more input neurons can be used, and still only two output channels are needed. Two levels of monitoring are possible using the SNS; a coarser SHM approach, or an on-board NDE approach.

*Author to whom correspondence should be addressed.
E-mail: Goutham.Kirikera@northwestern.edu
[†]Work performed at SSBNL in University of Cincinnati
Figures 1–13 appear in color online: http://shm.sagepub.com

Vol 7(1): 0065–19
[1475-9217 (200803) 7:1;65–19 10.1177/1475921707081971]

The SHM approach uses the SNS with a coarse grid of neurons to monitor and detect damage occurring in a general area during operation of the structure. The SNS will indicate where and when a more sensitive inspection is needed which can be done using ground-based NDE techniques. The on-board NDE approach uses the SNS with a fine coverage of neurons for highly sensitive NDE which continuously listens for damage and provides real-time processing and information about any damage in the structure and the performance limits and safety of the vehicle.

Keywords structural neural system (SNS) · acoustic emission (AE) · structural health monitoring (SHM) · damage diagnostics and prognostics · real-time monitoring

Terminology used in this study

Continuous sensor: Interconnected piezoelectric ceramic sensors connected in series to form a long sensor. Different types of discrete sensors (e.g., pressure, temperature, acceleration) can also be used to form a continuous sensor.

Data acquisition channel: A signal processing board that converts analog signals to digital signals at a high sampling rate.

Firing: Firing is passing a signal when a threshold condition is met. This is similar to firing of neurons in the biological system. Firing occurs when the structural neural system analog processor (SNSAP) produces a unique DC voltage because the acoustic emission (AE) waveform has crossed the threshold voltage. This preset unique DC voltage can be unique for each neuron in the health monitoring network. The SNSAP has two analog output channels ($T1$ and $C1$ channel). The analog signals from SNSAP are converted into its digital form using a National Instruments data acquisition board and LABVIEW software.

Neuron: The combination of one continuous sensor and the individual electrical circuitry in the SNSAP to control the signal processing for each sensor/continuous sensor.

SNS: The structural neural system (SNS) is a sensor network that mimics the biological neural system to locate damage on large complex structures in real time. The SNS is a combination of many sensors and the SNSAP. The SNS remarkably reduces the overall number of data acquisition channels needed for successful real-time SHM.

SNSAP: The structural neural system analog processor is the electronics hardware that is analogous to the soma or cell in the biological neural system. The SNSAP collects signals from many sensors and produces only two analog output signals to predict the damage location and approximate severity.

Threshold voltage: The voltage level at which the neurons fire and the signals are collected for damage detection analysis. Any AE waveform signal with amplitude greater than the threshold voltage is processed by the SNSAP. Unique preset DC voltage signals corresponding to each neuron are fired by the SNSAP.

Damage: Cracks or delamination. In this study, the damage is caused by fatigue. Acoustic emissions are released due to damage growth.

1 Introduction

Structural health monitoring (SHM) of aerospace, civil, and other structures is an important need, and two different general types of health monitoring methods are currently being developed. The first is the active structural health monitoring (ASHM) method for maintenance on-demand/condition based monitoring in which actuators are used to pulse the structure with a known waveform. The resulting stress waves propagating in the structure are used for detecting damage. A number of researchers have been using this method for damage prognostics and diagnostics [1–5]. The ASHM methods generate diagnostic signals and map wave propagation to detect damage. The second method is the passive structural health monitoring (PSHM) method for real-time health monitoring in which stress waves due to propagation of cracks or other damage are sensed and analyzed. These stress waves are conventionally called an acoustic emission (AE).

AE is the elastic energy that is spontaneously released by materials when they undergo crack initiation and propagation [6]. Crack propagation in metallic and composite structures is accompanied by AE. Years of research in AE has produced reliable offline algorithms for diagnostics and prognostics [7–14]. However, using AE for PSHM has been limited by the large size of the sensors and the need for a large number of channels of data acquisition.

Some details of wave propagation in structures are provided next before discussing the approach for damage detection proposed in this study. In thick sections of structures, longitudinal, shear, and surface waves can propagate and the velocity of the wave depends only on the type of material. When the wavelength of the propagating waves is on the order of the thickness of the structure in consideration (a thin section), Lamb waves propagate in the structure with multiple wave modes. Damage localization is mainly performed based on the change in wave speed due to the growth of damage. Lamb waves are very useful as they can travel long distances and they are currently widely used by the health monitoring community for diagnostic purposes. It is well known that Lamb waves are dispersive and the wave speed changes with respect to the geometry/shape of the structure, the material properties, and the frequency of the propagating waves. Hence, for complex structures consisting of fasteners, ribs, joints, or heterogeneous materials, damage localization based on wave speed may not be efficient for real-time SHM. Real-time SHM should be autonomous and if possible not require elaborate artificial intelligence (e.g., wave propagation structural models, artificial neural network analysis, nonlinear dynamics, genetic algorithms, etc.) to process the data to indicate the existence of damage.

Lamb waves in thin aerospace structures are ultrasonic waves that propagate differently when compared to longitudinal and shear waves [15]. The velocity of Lamb waves depends on the material, geometry, and frequency [15]. The wave modes of the Lamb waves are dispersive, and hence multiple wave velocities can exist in the signal. In addition, multiple wave modes can exist at a particular frequency of interest. The wave structure of the fundamental mode also changes its polarization direction as the frequency changes in the dispersion curve [8,15]. Acousto-ultrasonic techniques are based on active wave propagation and generate guided ultrasonic stress waves using a set of actuator and sensor piezoelectric wafers. The high-frequency excitation and interaction with the structure produces a large number of mixed wave modes and the sensor responses contain directly propagating wave modes and reflected and scattered modes. Damage detection using the time of flight or wave propagation mapping methods, either in an active or passive approach, is commonly used. But using this technique with multiple wave modes and frequencies (i.e., in complex structure geometries with high feature density) can lead to an erroneous result in detecting the existence and location of damage [8]. In flat isotropic/composite plates that are conventionally tested in laboratory environments, and based on prior knowledge of the material properties and geometry of the material, damage can be identified using the time of flight methods. But this may not be an efficient approach for real-time SHM of realistic large complex structures that exist in the field.

For ASHM based on Lamb wave propagation or the acousto-ultrasonic method, any discontinuity in the structural geometry or material will change the wave propagation characteristics. This means that many closely spaced sensor and actuator pairs may be needed to detect small damage, and pre-damage data must be stored and compensated for any environmental changes or aging of the structure. Small growing damages are very difficult to find using ASHM unless the excitation frequency is very high, on the order of MHz. If the excitation frequency is high then large numbers of sensors are needed to be placed close to each other as high frequency waves tend to attenuate faster.

For PSHM based on AE analysis, such as triangulation, wave propagation in complex geometry affects the accuracy of locating damage, but not so much the detection of damage. Numerous researchers have performed analytical modeling of AE. In particular Hamstad et al. [11,16], using the finite element technique, has shown that a buried dipole source represents more closely the AE rather than the lead break surface monopole source.

However, for experimental validation of sensor system prototypes, lead breaks on the surface need to be used. Prosser et al. [10] using a calibrated, wideband, conical element sensor has shown that a lead break on the surface preferentially generates the A_o mode compared to the S_o mode. Similarly a pencil lead break on the plate edge (concentrated on the midplane) preferentially generates the S_o mode compared to the A_o mode. Also it is shown [10] using a calibrated, wideband sensor that an S_o mode consists of high frequency components compared to the A_o mode. Based on the above information, it is clear that damage generates different type of modes depending on the geometrical location of damage, thus complicating the wave propagation analysis. But the type of damage might also be inferred based on the waveform characteristics. Significant work summarized below has been done to understand AE propagation.

Gorman [8], Prosser et al. [9,10], Hamstad et al. [11–13,16], and Dunegan [14] performed considerable work characterizing Lamb waves that form AE signals in thin plates. Gorman [8] and Prosser et al. [9,10] show that the source orientation has a considerable effect on the type of waves produced. A pencil lead break on the surface and edge of a plate was used to simulate AE waves due to damage. Apart from the generation of the fundamental modes, there exists also a Rayleigh wave which propagates along the edge of the plate for the edge pencil lead break. The interaction of the Rayleigh wave with the plate corner produces a mode converted S_o wave. The shear waves caused by the edge break source interact with the sides of the plate to produce longitudinal waves upon reflection, which then propagate through the thick plate as the S_o mode. Use of this mode in direction localization would induce considerable error in the damage location. In general, monitoring waves as they propagate from the source in a complex structure becomes increasingly difficult the farther the sensor is from the source. Damage detection could be improved by a simple real-time diagnostic method that eliminates complex wave propagation analysis.

Recently, there have been considerable advances in developing simple and rugged piezoelectric, MEMS, and optical fiber sensors [4,17]. But there has been little advancement done in the field of data acquisition and simplifying the huge amount of data that are acquired to predict the location of damages. The cost of the A/D converters is high due to the high sampling rate or the large number of channels to monitor large number of static strain sensors. Thus, installation of a large number of data acquisition channels can be cost prohibitive for SHM.

This study proposes a real-time passive method for damage detection based on sensing waves or AE produced by damage. The sensor network is called a SNS and it is based on the signal processing done in the human biological neural system. Similar to the human biological system, the passive SNS is typically on all the time and listens for any damage growing in the structure. Reduction of the complexity of the sensor system and investment in data acquisition, and simplifying the data reduction and analysis [18] are the driving force behind the development of the SNS [19]. The SNS uses long continuous sensors that are close to damage and are not adversely affected by the multi-mode Lamb wave dispersion phenomenon. This SNS uses analog logic circuits that mimic the way the biological system propagates signals. The biomimetic architecture tremendously reduces the number of high sampling rate channels that are conventionally required to monitor AE. To verify the SNS concept, a small prototype system was built and tested. This study shows results of using the SNS to monitor in real time the damage growth in a composite specimen during fatigue testing. The first section of this study gives a brief description of the architecture of the SNS followed by an overview of the current status of research in SNS development, and then an introduction to the experimental setup. The study concludes by presenting the results for damage localization using the real-time SNS approach.

2 Architecture of the Structural Neural System

Figure 1(a) shows the architecture of the SNS on a large panel depicted by the large square. Each small square indicates two sensors placed

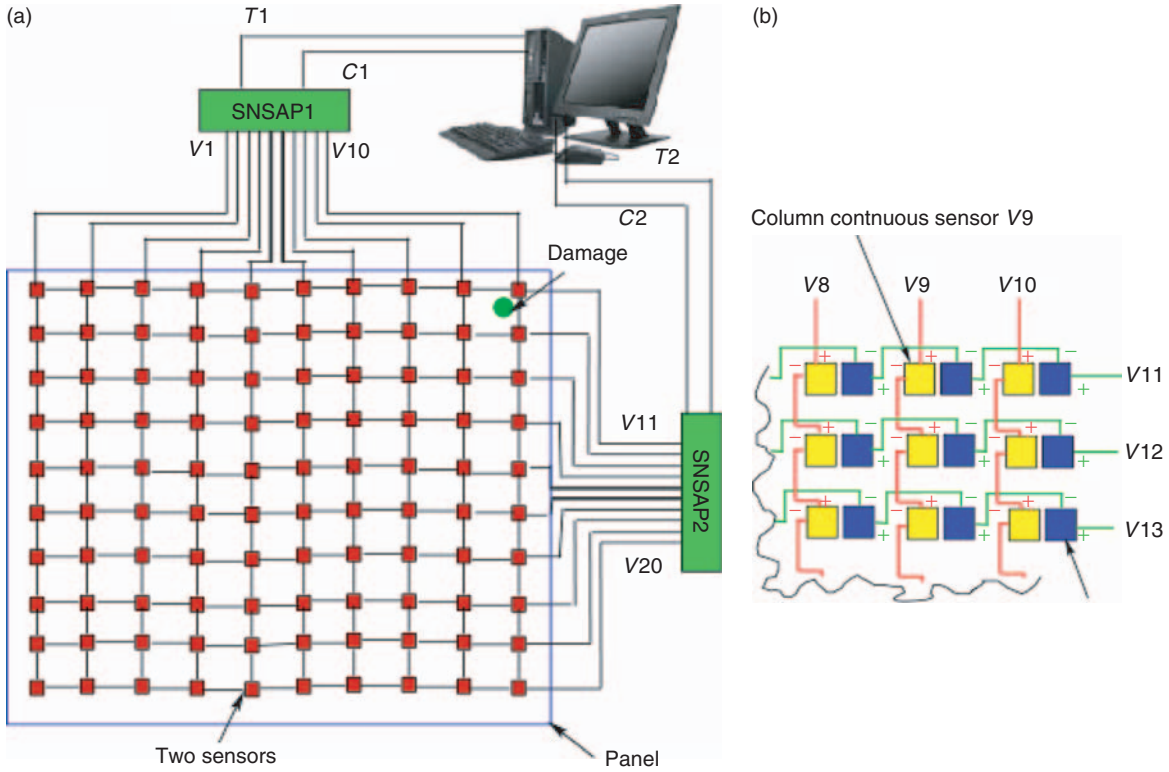

Figure 1 Architecture of the structural neural system: (a) Each small square indicates two adjacent sensor nodes. There are 200 sensors in Figure 1(a). Circuits *V*1 through *V*20 contain 20 analog output signals from the continuous sensors. SNSAP1 and SNSAP2 are two analog processors built to simplify the damage location process. *T*1, *C*1, *T*2, and *C*2 are the four output signals sent to the computer. Software for damage detection is written using MATLAB and LABVIEW to acquire and analyze the data and (b) zoomed version of Figure 1(a) showing details of arranging sensors to form row continuous sensors and column continuous sensors.

next to each other but not connected to each other (larger view shown in Figure 1b). One of the sensors at this location is connected in series to other sensors located in a horizontal row (Figure 1b). This type of connection is called a continuous sensor [20]. The connection of multiple sensors in series will not affect the response of the individual sensors to acoustic emissions provided each piezoelectric element in the continuous sensor has the same sensitivity. A total of 16 PZT sensors [27] can be connected in series to form a continuous sensor without degrading the signal to noise ratio of the signal. The second sensor located adjacent to the first sensor is connected in series to the sensors located in a vertical column (Figure 1b). The output signals from the column continuous sensors are labeled *V*1–*V*10, and the output signals from the row continuous sensors are labeled *V*11–*V*20, as shown in Figure 1(a). Using the continuous sensor architecture, the large health monitoring grid containing 200 individual sensors is reduced to just 20 output channels (*V*1 through *V*20). The aim of the SNS is to minimize the number of data acquisition channels, but still predict the location of damage. To achieve this, a SNS analog processor (SNSAP) is built using commercially available analog electronic components such as resistors, capacitors, transistors, and operational amplifiers. The outputs of the continuous sensors (*V*1 through *V*20) are input to the SNSAP1 and SNSAP2 as shown in Figure 1(a). The continuous sensor and the individual electronic circuitry in the SNSAP corresponding to each continuous sensor are called a neuron. The output of SNSAP1 consists of only two analog time signals (*C*1 and *T*1 in Figure 1a) even though the health monitoring network consists of a large number of sensors. Similarly the output from the

row continuous sensors ($V11$ through $V20$) is sent into SNSAP2 and the resulting analog time signals are $C2$ and $T2$. These four analog time signals ($T1$, $C1$, $T2$, and $C2$ in Figure 1a) are converted into digital form using a high sampling rate National Instruments data acquisition board. LABVIEW and MATLAB algorithms were developed to perform the data acquisition and determine the location of the damage.

Damage is located using the architecture of the SNS, shown in Figure 1(a). The circle in this figure illustrates damage on the plate. As the damage progresses during operation of the structure, high frequency AE stress waves are released. In this illustrated example, since the AE is close to continuous sensors $V10$ and $V11$, a response occurs first in these continuous sensors. These signals are sent into SNSAP1 (through $V10$ initially) and SNSAP2 (through $V11$ initially). A threshold voltage is selected by the user based on the application. Any AE waveform amplitude that exceeds this threshold voltage causes the SNSAP1 and SNSAP2 to fire a unique preset DC voltage corresponding to continuous sensors $V10$ and $V11$, respectively. Firing is the generation of a unique preset DC voltage signal by the SNSAP corresponding to a continuous sensor. As the AE waveform progresses in the plate, other continuous sensors fire sequentially ($V9$, $V12$, $V8$, $V13$, etc). Because of damping in the structure and the existence of a high pass filter in the SNSAP, only signals corresponding to a particular threshold value and frequencies of the order of 100 kHz are analyzed in the SNSAP. $T1$ and $C1$ are the outputs of SNSAP1. $T1$ consists of combined time domain AE waveforms of the firing neurons in the health monitoring network. A neuron is the combination of a continuous sensor and its corresponding electrical circuit present in the SNSAP. Similarly $C1$ consists of unique preset DC voltages that identify the propagation of waves as they travel over the neurons in the structure. $T2$ and $C2$ are the corresponding outputs of SNSAP2. The four output channels $T1$, $C1$, $T2$, and $C2$ are sent into a data acquisition computer for further analysis. Algorithms written in MATLAB and LABVIEW are used for data acquisition and damage localization. These programs decode the signal in the $C1$ channel to identify which neurons are firing. The firing information along with combined AE waveforms in the $T1$ channel are used to locate the damage within one grid of the pattern of continuous sensors. Thus, with many sensor nodes, only four channels of data acquisition (conversion from analog to digital mode) are required to locate and qualitatively determine the severity of the damage.

The advantage of the SNS is that the system is mostly analog and this eliminates the many channels of data acquisition or multiplexers with high sampling rates that are conventionally required. In addition, the SNS system is user-friendly and damage is easily located by the order of firing of the neurons. The same SNS can be used for both PSHM and ASHM. PSHM involves the detection of stress waves produced due to the progression of damage. ASHM (not tested in this study) involves excitation of the structure using an actuator and comparing the firing pattern from the SNSAP for the healthy structure to the firing pattern from the SNSAP for the damaged structure. To demonstrate the concept of the SNS, a prototype consisting of four sensor inputs was built and the results of damage diagnostics during fatigue testing using only passive health monitoring are shown in this study.

3 Previous Studies of Damage Detection Using the SNS

Previously a two-neuron first prototype of the SNS was designed and built. Results of testing the passive SNS two neuron prototype are given in [21,22]. There were two limitations in the analog electronics in the first prototype SNS; the response of the electronic components was slow, and the electronics needed shielding. To overcome these problems, the SNSAP was designed with much faster electronic components and also better electronic shielding. In addition, to prove that the system is practical on a larger scale, the two neuron prototype was extended to a four neuron prototype. Results of testing the four neuron prototype on a thin composite plate in a laboratory controlled environment was reported in [23].

In addition, to understand the propagation of Lamb waves on a thin plate, a wave simulation

algorithm has been under development [22,24]. The wave simulation algorithm is derived using the modal superposition method and is based on the classical thin plate theory. The wave simulation algorithm was extended to excite a composite structure using an actuator at a specific frequency. The group velocity of the fundamental lower order asymmetric Lamb wave mode was compared and agreed satisfactorily with the group velocity obtained through the classical thin plate theory for an isotropic plate [25]. Long continuous piezoelectric sensors were recently modeled in the wave simulation algorithm to study the ability of continuous sensors to detect acoustic wave propagation [26].

4 New Results Presented in this Study

The major focus of this study is to validate the SNSAP architecture for real-time passive SHM and for future scale-up. The new developments presented in this study are: (i) a simple four neuron prototype SNS was built, (ii) the system was tested on a composite panel undergoing fatigue cycling, and (iii) a damage detection algorithm was developed based on the signal outputs from the SNS. Results of the testing are reported for the first time in this study. This article mainly focuses on detecting the location of damage using the passive SNS during real-time fatigue testing of a composite panel loaded on a four-point bending fixture in a mechanical testing (MTS) machine. Four piezoelectric sensors were bonded on the surface of the specimen. The outputs of the four sensors were used as inputs to the SNSAP. The architecture of SNSAP has two output channels irrespective of the number of sensors used as inputs. In this case, the prototype SNSAP has four sensor inputs and two channels of output. One of the output channels tracks the propagation of waves over the composite specimen for the whole test duration by firing a unique signal corresponding to each sensor. The other channel contains the combined time domain response from all the neurons. The signals from the two channels are captured and stored in digital form using a program written in LABVIEW. The signal obtained using the LABVIEW program is decoded using a MATLAB algorithm and used to predict the damage location. Thus, with just two digital channels of data acquisition, and using the concept of firing of the neurons, propagating stress waves can be tracked in the structure in near real-time.

Note that in Figure 1(a) the basic concept of the SNS was explained using 10 column continuous sensors ($V1$–$V10$) and 10 row continuous sensors ($V11$–$V20$). The output of these 10 column continuous sensors is sent as input to SNSAP1 and similarly the output of 10 row continuous sensors is sent as input to SNSAP2. A small prototype of SNSAP consisting of four input channels was designed and tested in this study to prove that the concept of SNSAP is practical and feasible. In addition, only individual sensors were used in this testing. The architecture of continuous sensors has been tested elsewhere [27–29].

5 Experimental Setup and Fatigue Testing

A flat coupon 1.25 cm (0.5 in.) thick and 8.0 cm (3.15 in.) wide was cut from a large orthotropic plate of glass fiber woven composite material. The plate has approximately 60% volume fraction of fibers. The plate was fatigued using a four-point bending specimen at 3 Hz with a large mid range stress and a moderate alternating stress corresponding to an alternating displacement of the fixture of 2 mm. Figure 2(a) shows the test setup for this experiment. Figure 2(b) shows the dimensions of the 1.25 cm thick composite plate used for this test. Four sensors were placed on the surface of the composite to monitor the damage growth process. The sensors were located at a distance of 30.5 mm (Sensor 1), 152.4 mm (Sensor 2), 222.3 mm (Sensor 3), and 260.4 mm (Sensor 4) measured from the left end of the loading point shown in Figure 2(b). To accelerate the damage growth in the specimen, a notch 11 mm long with a depth $<$1 mm was put on the surface of the plate between Sensors 1 and 2, but closer to Sensor 2 than to Sensor 1. As the damage grew through the plate, high frequency AEs occurred. These emissions were used as input to the SNSAP to detect the location of damage in the composite specimen.

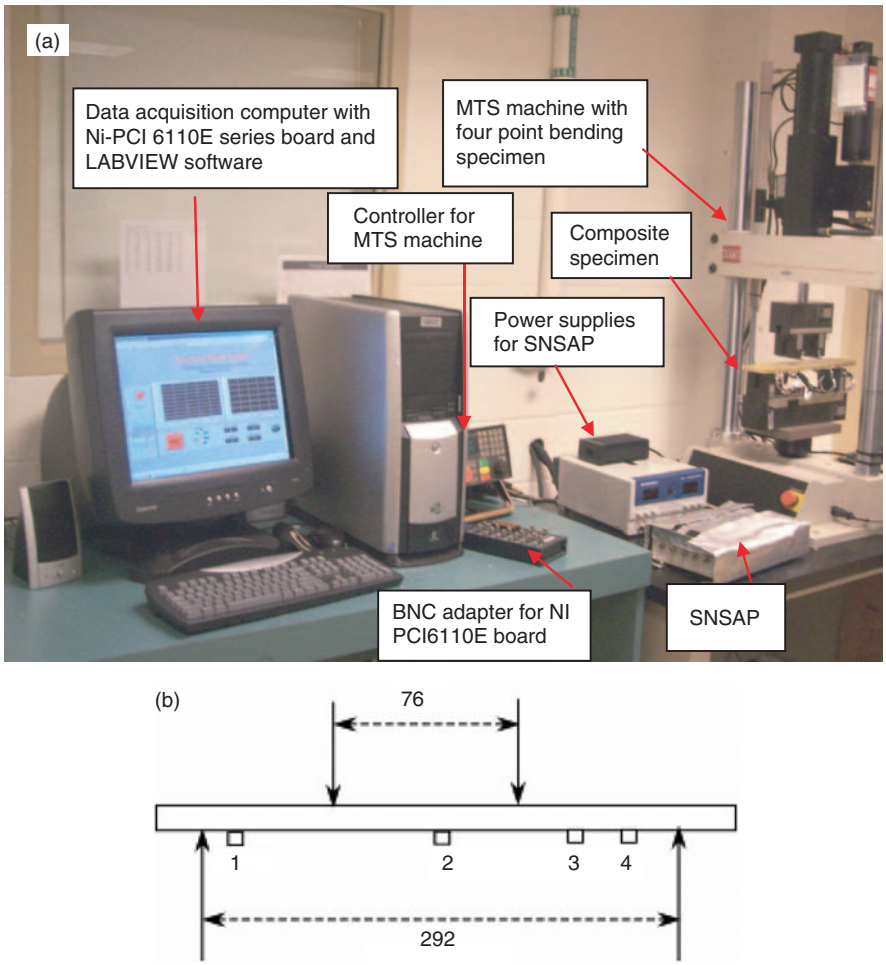

Figure 2 Testing of a composite specimen under four-point bending load: (a) test setup and (b) the 1.25 cm thick composite test plate with four sensors (1, 2, 3, and 4). Dimensions in the figure are in mm.

The composite specimen was loaded using a four-point bending specimen as shown in Figure 2 and fatigued for a total of 92,957 cycles at the rate of 3Hz. The displacement applied to the composite beam using the MTS machine is shown in Figure 3(a) as a function of the number of fatigue cycles. The digital controller used to control the motion of the loading points also indicates the maximum load applied to the specimen. The variation of applied load as a function of number of cycles is shown in Figure 3(b). AE hits were recorded during the test as the crack started growing in the plate. The number of AE hits (occurrences) recorded during the test is shown in the right axes of Figure 3.

The crack length at different stages of testing is shown in Figure 4. The corresponding number of fatigue cycles and hits are given in Table 1. At ≈92,521 cycles the length of the crack due to fatiguing of the plate was 31 mm on one side of the initial damage, and 21mm on the other side of the damage. Figure 4 indicates that at 92,521 cycles the damage that has been progressing on the surface of the specimen has reached one edge of the plate. At 92,957 cycles the crack length as shown in Figure 4 is 31 and 38 mm on the sides of the initial 11 mm damage, and has reached both edges of the plate. The crack growth information is summarized in Table 1. Figure 5 indicates that the crack traveling through the thickness of the plate (at a 5mm depth) has started to delaminate of the plate. The delamination started probably because of transverse shear at the crack free edges. The SNS monitors the AE rate and indicates

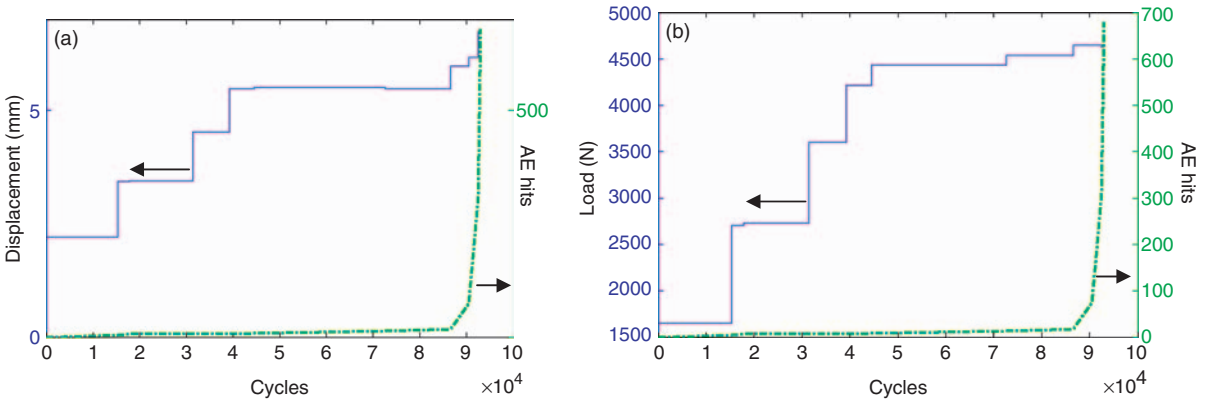

Figure 3 AE profile along with: (a) panel displacement and AE hits and (b) load and AE hits as a function of number of fatigue cycles.

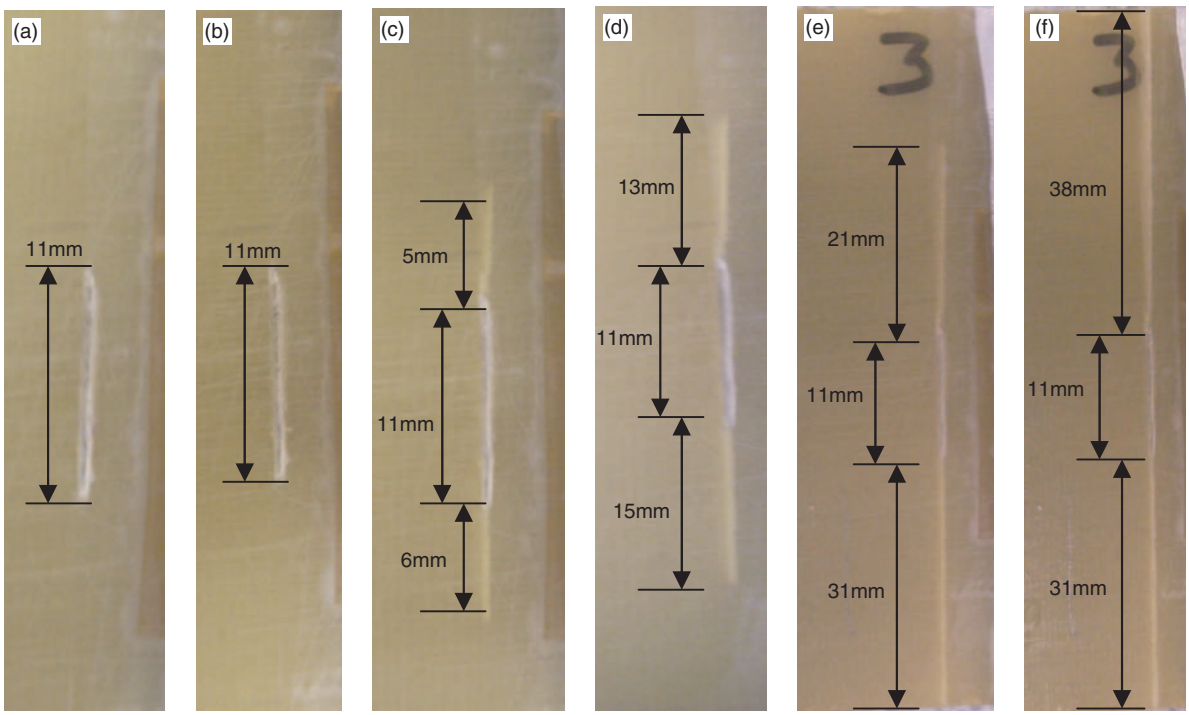

Figure 4 Crack length at different stages of fatigue testing as defined in Table 1.

when the rate starts to increase, in this case at about 87,000 cycles. At this time a warning would be issued to the operator or pilot stating that the loading must be reduced and the damage must be repaired immediately. This experiment was designed to represent a case of severe unanticipated damage to the material or aircraft or other structure and illustrates that under high loading, damage can propagate fast and real-time passive monitoring methods like SNS can detect damages in time to prevent failure. The next section of this study demonstrates the real-time health monitoring capability of the SNS.

6 Data Acquisition Using the SNS

The SNS was used to monitor the AE produced due to cracking of the composite. Four lead zirconium titanate (PZT) sensor nodes were

used as four independent sensors to test the architecture of the SNSAP. A PZT sheet of dimensions $(72.4 \times 72.4 \times 0.3)$mm was cut using a sharp razor blade into $(15 \times 5 \times 0.3)$mm wafers. Copper strips were attached to the wafer using EPO-TEK's H20E silver conductive epoxy. The wafer and the silver conductive epoxy were heated in an oven at 150°C for 2 h to cure the epoxy. A Kapton sheet was used to insulate the wafer from the surroundings. These wafers were bonded onto the surface of the composite using superglue. A thin aluminum foil was wrapped around the bonded sensor and grounded. The sensor was attached so that the long side of the sensor was parallel to the width of the composite plate, as shown in Figure 6. This allows sensing of high frequency waves traveling along the length of the panel. Waves reflecting from the boundaries of the composite would tend to travel along the length of the sensor and thus be partially spatially filtered out of the response because the length of the sensor is greater than the length of the waves. In practice, a large number of individual sensor nodes can be connected in series to form a continuous sensor. The gain in the charge amplifier of the SNSAP needs to be adjusted to compensate for the decreased capacitance as a result of multiple sensors being connected in series. The outputs of the four

Table 1 Summary of fatigue testing results.

Number of fatigue cycles	*Maximum load (N)*	*Number of AE hits*	*Crack length (mm)*	*Figure with crack*
15,333	1650	5	11	4(a)
31,434	2731	7	11	4(b)
86,557	4537	18	22	4(c)
90,541	4648	75	39	4(d)
92,521	4646	307	63	4(e)
92,957	4628	679	80	4(f)

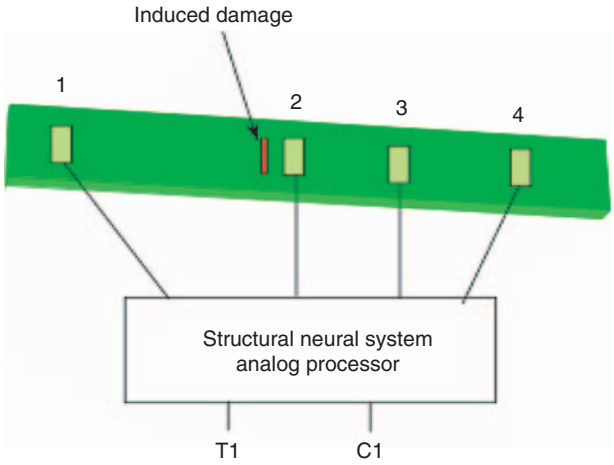

Figure 6 Geometry of the composite specimen with sensors and the SNSAP.

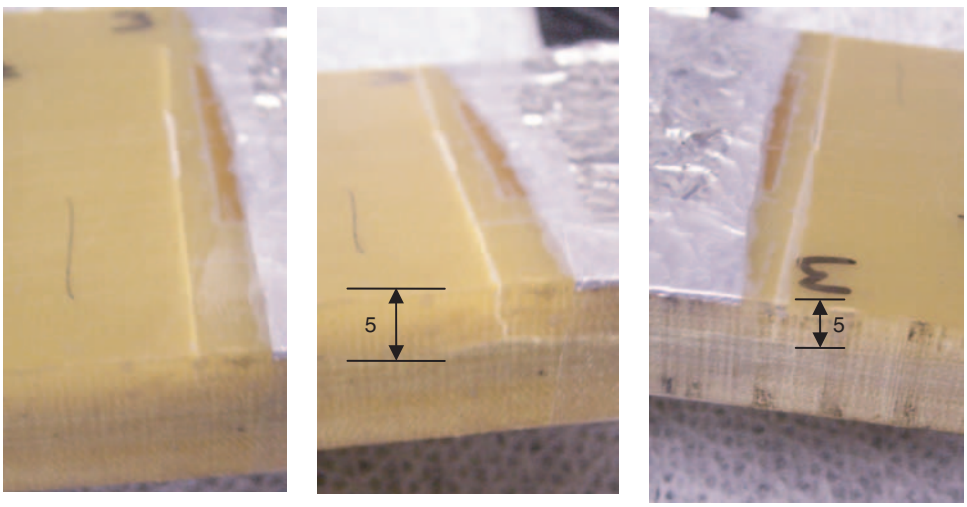

Figure 5 Through the thickness damage with respect to the number of fatigue cycles.

sensors were sent as inputs to the SNSAP shown in Figure 6. The outputs of SNSAP are $T1$ and $C1$. $T1$ indicates the time domain combined response of all the sensors and $C1$ tracks the propagation of waves on the composite with respect to the sensors. $T1$ and $C1$ were also earlier referenced in Figure 1(a).

Figure 7 shows the gain of the SNSAP due to the analog circuitry and the phase difference between the output of the sensor and the output of the SNSAP. Initial testing was done for about 70,000 fatigue cycles and then the gain and the cutoff frequency for the high pass filter in the SNSAP were changed to capture lower amplitude AEs. In practice, it is anticipated that the SNS filtering would be configured for each specific application. The gain and the phase plots were obtained experimentally by exciting the plate at steady state through varied discrete frequencies. The data obtained by connecting the output of the sensor across the oscilloscope are compared with the data obtained from the sensor connected to the SNSAP which in-turn is connected across the oscilloscope. Using this method, the gain and phase of the SNSAP were calculated eliminating the dependence of the obtained data on the material properties, number of modes excited, dimensions of the structure, location of excitation and receiver, and the individual amplitudes of the various modes. MATLAB's basic fitting tool guide was used to fit the experimentally obtained curves. The maximum gain as obtained experimentally is at 65 kHz with 40.74 db gain. The phase difference between the raw sensor output and the output of the SNSAP at 65 kHz is -164.03° (obtained experimentally). This indicates that the output of the SNSAP lags the sensor signals.

Figures 8 and 9 show the response of channels $C1$ and $T1$ of the SNSAP for fatigue testing that lasted for $\approx$8.7 h. The SNSAP assigns a unique preset voltage for each neuron. When the neuron senses the propagating AE wave which crosses a preset fixed threshold voltage, the SNSAP generates an analog signal with a unique preset firing voltage corresponding to that particular neuron. A threshold of 0.4 V was selected for this particular fatigue testing. The selection of this threshold is dependent on the structure. Pencil lead breaks (a standard way to simulate AE) were used before the actual testing to determine this level. Thus, the combination of all the AE waveform signals ($T1$ channel) and the preset unique voltage signals ($C1$ channel) of all sensors is converted into digital form and stored in a computer using a LABVIEW based program. To simplify the process of tracking the propagation of AE waves through channel $C1$, a MATLAB algorithm is written that converts the unique voltage assigned to each neuron into the respective neuron numbers as referenced in Figure 6 (Neurons 1, 2, 3, and 4). The neuron firing is displayed in Figure 8(a). This figure indicates the corresponding time at which

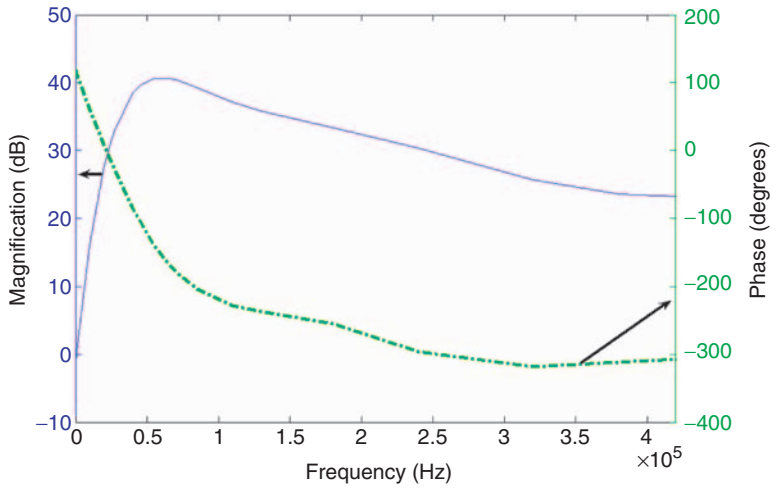

Figure 7 Magnitude and phase of the SNSAP.

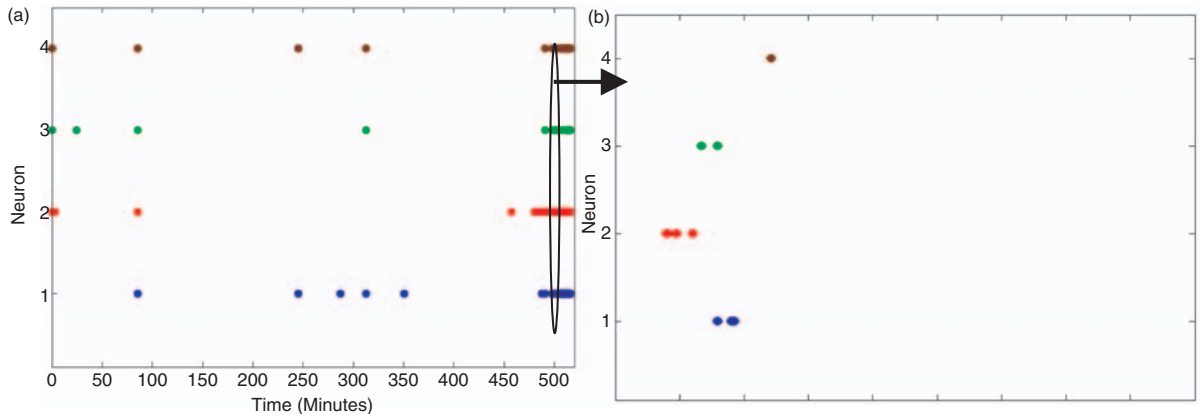

Figure 8 Response of channel *C*1 of the SNSAP: (a) overall response for the test and (b) zoomed version of Figure 8(a) obtained at the 490.75th minute. This corresponds to the 35th AE captured by the SNSAP. A total of 500 data points are plotted with a sampling rate of 1×10^6 samples/sec.

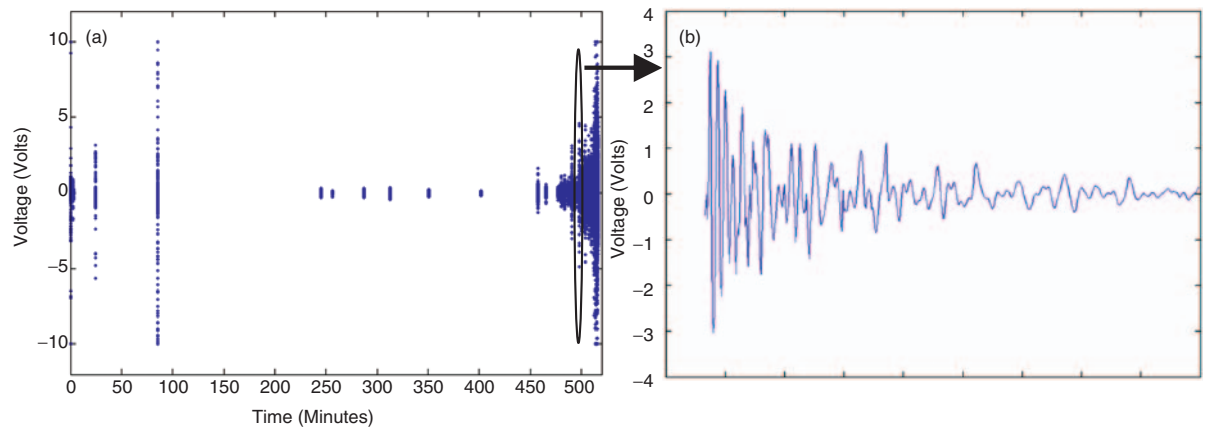

Figure 9 Response of channel *T*1 of the SNSAP: (a) overall response for the test and (b) zoomed version of Figure 9(a) obtained at the 490.75th minute. This corresponds to the 35th acoustic emission captured by the SNSAP. A total of 500 data points are plotted with a sampling rate of 1×10^6 samples/sec.

each neuron has responded to the propagating AE wave. Figure 8(b) is a zoomed version of Figure 8(a) at the 490.75th minute (randomly picked). Figure 8(b) is similar to the simulation [22] performed earlier and indicates that AE wave tracking is indeed practical. Figure 8(b) indicates that Neuron 2 has fired first followed by the other neurons sensing the propagating AE. This indicates the AE was closest to Neuron 2.

Figure 9(a) displays the combined time response of all the neurons and corresponds to channel *T*1 as indicated in Figure 6. For every corresponding tracking of the neurons as displayed in Figure 8(a), Figure 9(a) consists of the high frequency AEs captured by the SNSAP. Figure 9(b) is the zoomed version of Figure 9(a) at the 490.75th minute indicating the high frequency content of the AE. Both Figures 8(a) and 9(a) are used to predict the location of damage.

7 Damage Detection Using the SNS

Damage is localized based on the neuron that first triggers the data acquisition software, although more than one neuron may receive AE signals due to the damage. For the full test, there were a total of 679 AEs and data files loaded in the data acquisition software. Each file contains 0.01 s of data at a spacing of 1×10^{-6} sec between each data point, as displayed

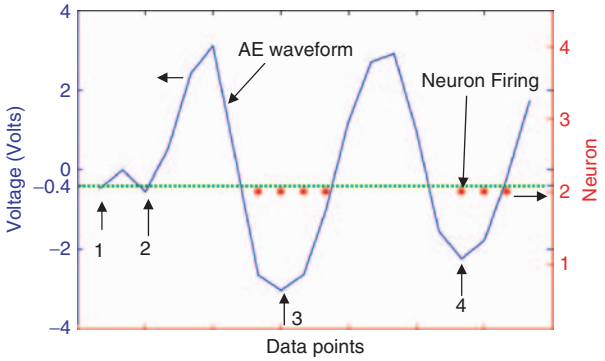

Figure 10 Zoomed version of Figures 8(b) and 9(b) indicating only the first 20 data points at a sampling rate of 1×10^6 samples/sec.

in Figures 8(a) and 9(a). Since the sensor closest to the AE will respond to the signal first, only the first 20 data points of each file are needed and were used to predict the location of the damage. Shown in Figure 10 are the first 20 data points of the 35th AE waveform acquired at a sampling rate of 1×10^6 samples/sec. The first 500 data points of the 35th AE are shown in Figures 8(b) and 9(b). There are two ordinates shown in Figure 10. The left ordinate corresponds to the combined AE waveforms of all the neurons (the $T1$ channel of the SNSAP) and the right ordinate corresponds to the neuron firing signal (the $C1$ channel of the SNSAP). A threshold voltage of $+0.4\,V$ is set in the SNSAP. Any AE waveform with amplitude $>+0.4\,V$ is processed by the SNSAP and a unique voltage corresponding to that particular neuron is generated by the SNSAP. In the future, a bridge rectifier may be used to allow analysis of the complete waveform instead of just the positive peaks. An inverting op-amp exists in the SNSAP. Hence the signal shown in Figure 10 is inverted by 180°. This indicates that AE waveforms with voltages $<-0.4\,V$ (indicated by a horizontal line in Figure 10) are processed by the SNSAP. The outputs of $T1$ and $C1$ are stored using a LABVIEW program. A LABVIEW trigger voltage (different than the threshold voltage) is set to acquire and store the analog signals $T1$ and $C1$ using the LABVIEW program. A LABVIEW trigger voltage of 0.8V is set to store the signals ($T1$ and $C1$ channel) in digital form. This trigger voltage is different from the threshold voltage set on the SNSAP. This trigger voltage is based on the minimum possible trigger value by the NI data acquisition board. Whenever the $C1$ channel of the SNSAP exceeds the trigger voltage, the LABVIEW program stores channels $C1$ and $T1$ in digital form for 0.01 s (10,000 samples). The data acquired by LABVIEW are analyzed using a MATLAB algorithm. The first step in the algorithm is to process the output of the C1 channel to decode the unique preset neuron firing voltages. The corresponding neuron firing chart is shown in Figure 10 where the dots indicate the times when the neurons are firing. In this particular case, only Neuron 2 is firing. The second step in the MATLAB algorithm is to store the voltages of the AE waveform corresponding to the time when each neuron is firing. Only the first 20 data points of the AE waveforms are analyzed as shown in Figure 10. This figure has four peaks labeled 1, 2, 3, and 4 that are of interest in this analysis. Data are only analyzed from Peaks 3 and 4 because Peaks 1 and 2 are too short to uniquely determine which neuron is firing, based on the current electronic components in the SNSAP. The time difference between the occurrence of the threshold voltage and the maximum peak is too small for the electronics to respond instantaneously. This limitation can be overcome by replacing the electronic components in the SNSAP with faster responding components. The dots in Figure 10 indicate the times at which Neuron 2 has fired. The voltages of the AE waveform are stored and summed for each neuron corresponding to the times at which the neurons are firing (red dots). Figure 10 clearly indicates that the AE response for the first 20 data points occurs only due to Neuron 2 as Neurons 1, 3, and 4 have not fired. If two neurons fire together, which usually does not happen and depends on the sensor spacing, then the corresponding amplitude obtained from the $T1$ channel is added to the cumulative response of both neurons. The cumulative voltages of all the neurons based on the 679 AE events are plotted in Figure 11.

Figure 11 shows the cumulative voltages of the neurons. Neuron 2 has the highest amplitude compared to Neurons 1, 3, and 4 indicating

that the damage exists near Neuron 2. In addition, Figure 11 qualitatively indicates that at approximately the 485th minute the slope of Neuron 2 increases drastically indicating that damage is growing quickly.

Figure 12 shows the amplitude of each neuron displayed in Figure 11 for different numbers of fatigue cycles. Figure 12 and Table 2 indicate that the damage is located near Neuron 2. The cumulative voltages in Figure 12 are summarized in Table 2 for the four neurons along with the crack length, number of cycles, and the number of AEs obtained during this phase. Neuron 2 has the highest cumulative voltage indicating that most of the AEs were generated near Neuron 2. As the length of the damage increases, the number of AEs and the cumulative voltage corresponding to Neuron 2 increase drastically. The cumulative voltages for Neurons 1, 3, and 4 may be caused by noise from the loading fixture. Once a neuron or neurons first fire, data are collected for 0.01 s before data from another AE event are considered. This sampling condition is based on the LABVIEW architecture. Since data are only collected for the first 20 data points in the AE waveform, this could be a limitation if multiple AEs occur within 0.01 s. In most cases, the AE occurrences are spaced apart and few emissions are missed. If needed, a faster LABVIEW board could be used to capture closely spaced AEs. This experimentation shows that the SNS predicts the crack location and qualitatively predicts the damage severity. The procedure could also be done in real time by processing each AE as it occurs. In applications, the number of neurons can be increased almost arbitrarily. Moreover, in the future, features of the AE waveform might be used to identify the type of damage.

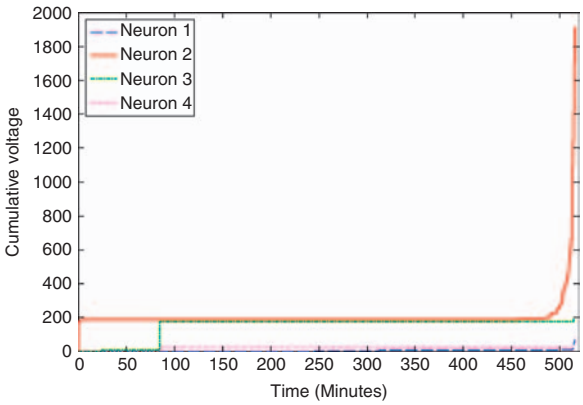

Figure 11 Individual sensor amplitude back calculated from the output of the SNSAP.

In this section, wavelet analysis is used to obtain the time–frequency representation of the AE signals. The time–frequency representation

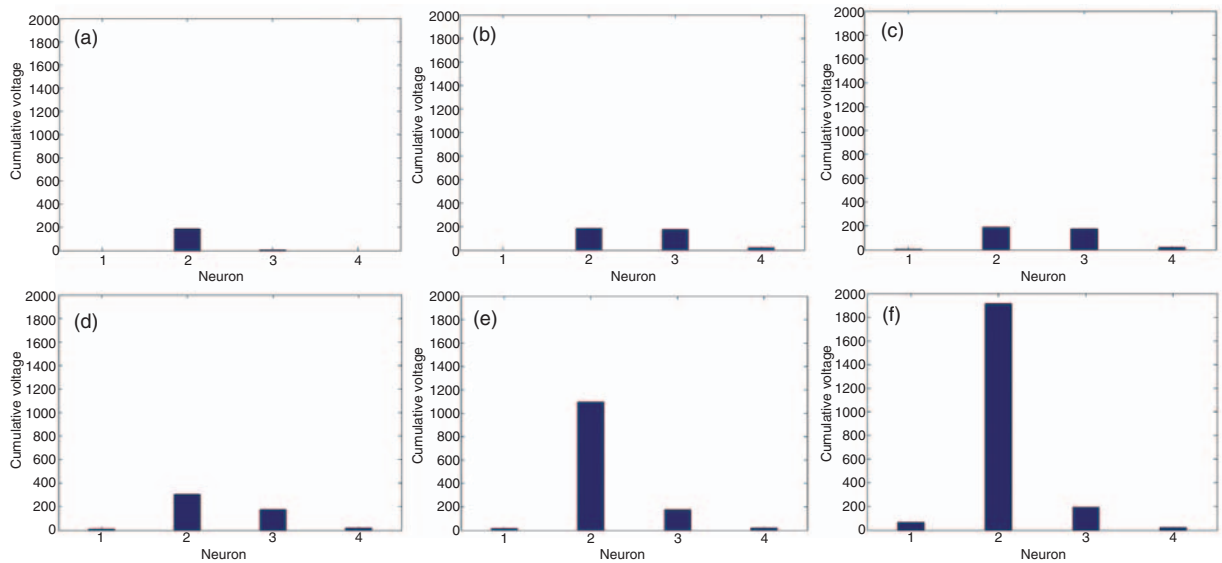

Figure 12 Damage location chart produced by reducing data obtained from the SNS. These figures were generated by SNS at the end of: (a) 15,333; (b) 31,434; (c) 86,557; (d) 90,541; (e) 92,521; and (f) 92,957 cycles.

shows features of the AE emissions that can help to design the SNS. The frequency and amplitude of the wavelet can help to determine the sensor size, spacing, and the filtering and gain in the SNS to obtain a good signal to noise level. Features of the wavelet might also be to characterize the type of damage that is occurring. For example, cracking and delamination may have different amplitudes and frequency content. Characterizing damage based on the AE waveform and the wavelet features is a subject of future work. Figure 13 shows three time domain AE signals from the test and the corresponding wavelet comparison. Acoustic emission numbers 35, 113, and 212 were chosen randomly from a total of 679 AEs obtained during this testing. Note the filtered and amplified signals have amplitude on the order of 3V and a good signal to noise ratio. As explained earlier, 679 AE files were accumulated during the testing. Each file was stored for 0.01 s at a sampling rate of 1e6 samples/s. The first 300 data points from randomly selected AE files (35, 113, and 212) were analyzed using the AGU-Vallen wavelet [12,13,30] software. A brief description of the wavelet transformation is given in [12,13,30–32].

Three random AE signals (35th, 113th, and 212th) were chosen from the database of 679 AEs. The sampling rate of the signals shown in Figure 13 is 1×10^6 samples/sec (Δt_s). There are a total of 1658 samples present in Figure 13. Only 300 samples of each AE file (35, 113, and 212) were considered and zeros were padded between each AE waveform. This was done to separate the AE waveforms in the time domain as shown in Figure 13. The abscissa in Figure 13 is time (μs) and the ordinate for wavelet transformation is frequency (kHz) and transient signals amplitudes are voltage (mV). The following parameters were used in the wavelet analysis; (a) the maximum frequency at which the wavelet transforms are computed was 500 kHz; (b) the frequency resolution was 1 kHz; and (c) the width of the wavelet is 500 samples. Different widths of the wavelet (200, 500, and 1000 samples) were tested and no significant difference was found between each of them. The analysis using 500 samples is displayed in Figure 13. The AE signals output shown in Figure 13 were in the range of 34–175 kHz with most of the dominant energy between 86 and 122 kHz. The energy of each signal is mainly dependent on the bandwidth of the SNSAP in addition to the sensor bandwidth and the number of modes excited by the source.

8 Summary and Conclusions

This study shows that the SNS can minimize the required number of data acquisition channels and predict the location of fatigue damage based on AE monitoring. Real-time continuous monitoring of a rectangular composite plate was performed. The composite specimen was loaded on a four-point bending fixture and the damage was monitored using four piezoelectric sensors. The output signals from these sensors are the inputs to the SNS analog processor, which has two analog output channels. One channel contains information for tracking the propagation

Table 2 Summary of damage detection results.

Number of fatigue cycles	*Crack length (mm)*	*Number of AE Hits*	*Figure*	*Neuron 1 (cumulative voltage)*	*Neuron 2 (cumulative voltage)*	*Neuron 3 (cumulative voltage)*	*Neuron 4 (cumulative voltage)*
15,333	11	5	12(a)	0	186	4	0
31,434	11	7	12(b)	0	186	174	0
86,557	22	18	12(c)	6	192	174	21
90,541	39	75	12(d)	8	304	174	21
92,521	63	307	12(e)	16	1095	174	21
92,957	80	679	12(f)	68	1915	195	23

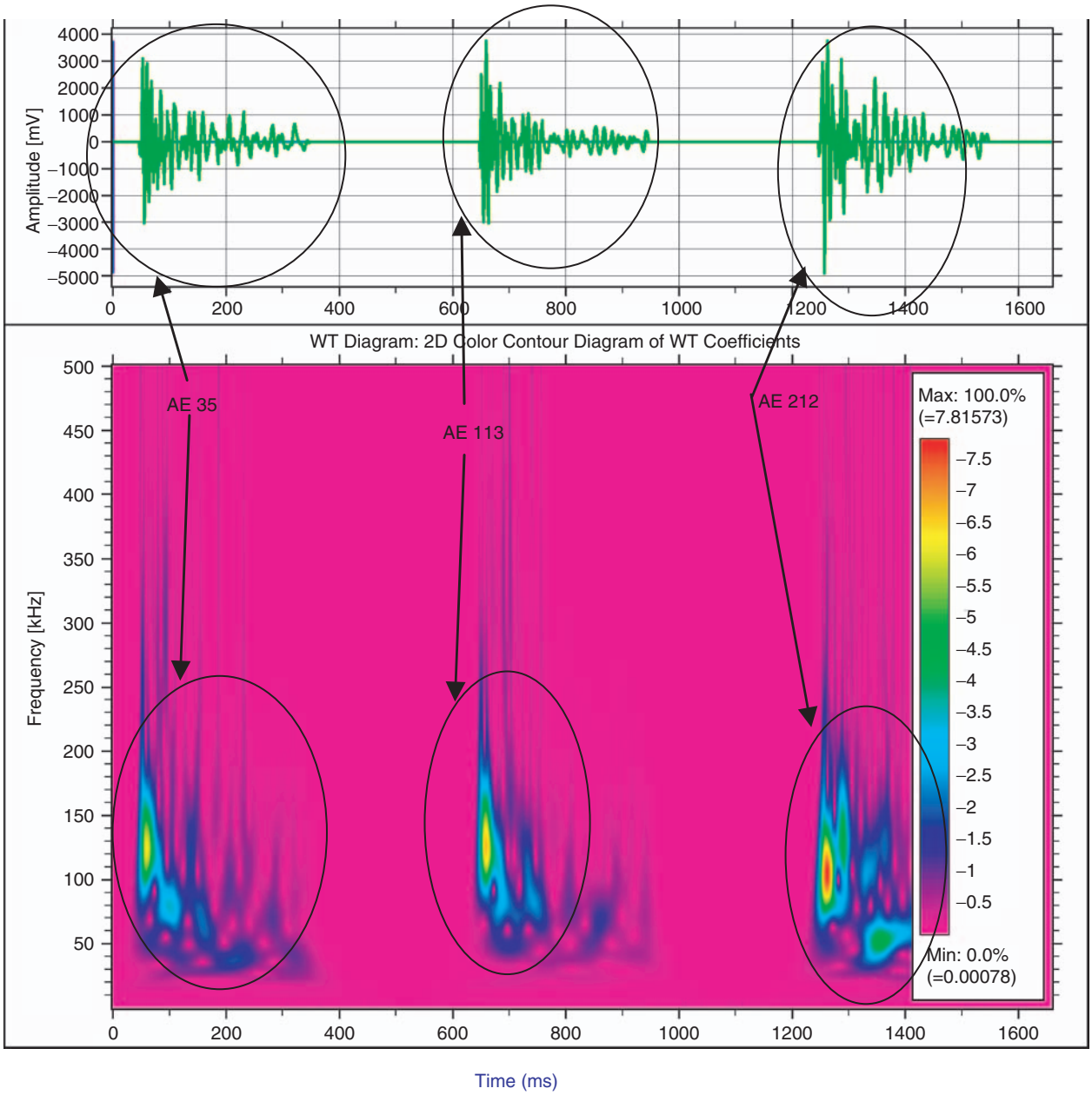

Figure 13 Wavelet transformation of acoustic emission signals obtained during fatigue testing. The abscissa is time (μs) and the ordinate for wavelet transformation is frequency (kHz) and transient signals amplitudes are voltage (mV).

of multi-mode Lamb waves. The other channel consists of time domain information indicating the frequency content of the waves.

The SNS was able to predict the location of damage using a diagnostic algorithm based on the neuron that fires first, which starts the data acquisition process. In addition, the cumulative AE voltage for each neuron was computed throughout the fatigue testing to qualitatively indicate the severity of the damage. Overall, a simple, practical health monitoring technique was developed that can predict the location of damage in real time. On a larger structure, the technique can be extended to use tens or hundreds of neurons each with many sensor nodes.

9 Future Research

The following work is currently being performed to make the SNS suitable for real time SHM

(a) Threshold limit: Currently the threshold for the SNSAP to fire is arbitrary. Further research needs to be done in selecting this threshold voltage. The threshold voltage depends on the thickness of the structure, spacing between the sensors, and the gain present in the SNSAP.
(b) Spacing between sensors: Spacing between the sensors is a very important concern for efficient SHM. In thick structures the spacing between sensors would be smaller. In thin structures, since waves can propagate long distances, the spacing between sensors can be large. Choosing the optimum spacing is structure dependent and requires further exploration.
(c) Continuous sensors: Real-time fatigue testing using continuous sensors is required to optimize the SNS to work for large continuous sensors.
(d) Field testing: The results presented in this study are from fatigue testing performed in a laboratory setting. Field testing of the SNSAP on large structures in the field would expose the potential advantages and disadvantages of the system.
(e) Large SNSAP: To predict the exact scalability and reduction in data acquisition channels, a much larger SNSAP needs to be built and tested. In addition, a bridge rectifier needs to be included in the future SNSAP.
(f) Damage characterization: Characterization of damage based on AE waveform and wavelet features is ongoing research with respect to SNS. For example, cracking and delamination may have different frequency content.
(g) Detection of multi-site damage: Detection of multi-site damage before final failure of the structure is important for practical SHM. Further field testing is required to explore this area.

Acknowledgments

This material is based upon the work supported by the National Renewable Energy Laboratory under subcontract number XCX-2-31214-01. Partial support of one author (G.R.K.) was through a summer fellowship received from University of Cincinnati, an assistantship by the Department of Mechanical Engineering at University of Cincinnati, and an educational scholarship in optics and engineering obtained from SPIE for the year 2005. Much of the help in making the prototype of the SNSAP was provided by engineers from Texas instruments and Analog Devices. Also Bo Westheider, Instrumentation specialist, and Doug Hurd, Machinist, in the Department of Mechanical Engineering at University of Cincinnati provided valuable tips in building the SNS prototype. All of the above mentioned support is gratefully acknowledged.

References

1. Park, H.W., Sohn, H., Law, K.H. and Farrar, C.R. (2006). Time reversal active sensing for health monitoring of a composite plate. *Journal of Sound and Vibration*, *302*(*1–2*), 50–66.
2. Giurgiutiu, V., Zagrai, A.N. and Bao, J.J. (2002). Piezoelectric wafer embedded active sensors for aging aircraft structural health monitoring. *Structural Health Monitoring*, *1*(*1*), 41–61.
3. Sundaresan, M.J., Schulz, M.J. and Ghoshal, A. (2002). Structural health monitoring static test of a wind turbine blade. March 2002, NREL/SR-500-28719, NREL Subcontractor Report.
4. Chang, F.-K. (2001). A summary report of the 2nd workshop on structural health monitoring. In: Prof. Chang, F.-K. (ed.), 3*rd International Workshop on Structural Health Monitoring*. *The Demands and Challenges*, Boca Raton, FL: CRC Press, pp. XXI–XLVI.
5. Kessler, S.S., Spearing, M.S. and Soutis, C. (2002). Damage detection in composite materials using Lamb wave methods. *Journal of Smart Materials and Structures*, *11*(*2*), 269–278.
6. Ness, S., Sherlock, C.N., Moore, P.O. and Mclntire, P. (1996). Nondestructive testing overview, *Nondestructive Testing Handbook*, Vol. 10, Columbus, OH: American Society for Nondestructive Testing.
7. Wells, R., Hamstad, M.A. and Mukherjee, A.K. (1983). On the origin of the first peak of acoustic emission in 7075 aluminum alloy. *Journal of Materials Science*, *18*(*4*), 1015–1020.

8. Gorman, M.R. (1991). Plate wave acoustic emission. *Journal of Acoustical Society of America*, *90*(*1*), 358–364.
9. Prosser, W.H. (1991). The propagation characteristics of the plate modes of acoustic emission waves in thin aluminum plates and thin graphite/epoxy composite plates and tubes. PhD Dissertation, NASA Technical Memorandum 104187, November.
10. Prosser, W.H., Hamstad, M.A., Gary, J. and Gallagher, A.O. (1999). Reflections of AE waves in finite plates: finite element modeling and experimental measurements. *Journal of Acoustic Emission*, *17*(*1–2*), 37–47.
11. Hamstad, M.A., O'Gallagher, A. and Gary, J. (2001). Effects of lateral plate dimensions on acoustic emission signals from dipole sources. *Journal of Acoustic Emission*, *19*, 258–274.
12. Hamstad, M.A., O'Gallagher, A. and Gary, J. (2002). A wavelet transform applied to acoustic emission signals. Part 1: Source identification. *Journal of Acoustic Emission*, *20*, 39–61.
13. Hamstad, M.A., O'Gallagher, A. and Gary, J. (2002). A wavelet transform applied to acoustic emission signals: Part 2: Source location. *Journal of Acoustic Emission*, *20*, 62–82.
14. Dunegan, H.L. (1997). Modal analysis of acoustic emission signals. *DECI Newsletters and Reports*, October.
15. Rose, J.L. (2003). Dispersion curves in guided wave testing. *Materials Evaulation*/January, 20–23.
16. Hamstad, M.A., O'Gallagher, A. and Gary, J. (1999). Modeling of buried monopole and dipole sources of acoustic emission with a finite element technique. *Journal of Acoustic Emission*, *17*(*3*/*4*), 97–110.
17. Derriso, M.M., Faas, P., Calcaterra, J., Barnes, J.H. and Sotomayer, W. (2001). Structural health monitoring applications for current and future aerospace vehicles. In: Prof. Chang, F.-K. (ed.), *3rd International Workshop on Structural Health Monitoring, The Demands and Challenges*, Boca Raton, FL: CRC Press, pp. 3–11.
18. Ghoshal, A., Prosser, W.H., Kirikera, G., Schulz, M.J., Hughes, D.J. and Orisamolu, W. (2003). Concepts and development of bio-inspired distributed embedded wired/wireless sensor array architectures for acoustic wave sensing in integrated aerospace vehicles. *4th International Workshop on Structural Health Monitoring*, Stanford CA, USA, 15–17 September, pp. 1161–1168.
19. Kirikera, G.R., Datta, S., Westheider, B., Schulz, M.J., Sundaresan, M., Martin, W.N. and Ghoshal, A. (2003). An artificial neural system with distributed parallel processing for structural health monitoring. *Invention Disclosure*, University of Cincinnati Intellectual Property Office, August 25.
20. Martin, W.N., Ghoshal, A., Sundaresan, M.J. and Schulz, M.J. (2002). Structural health monitoring using an artificial neural system. In: *Recent Research Developments in Sound and Vibration*, New Delhi, India: Transworld Research Network, pp. 373–408.
21. Kirikera, G.R., Shinde, V., Kang, I.P., Schulz, M.J., Shanov, V., Datta, S., Hurd, D., Westheider, B., Sundaresan, M.J. and Ghoshal, A. (2004). Mimicking the biological neural system using active fiber continuous sensors and electronic logic circuits. *SPIE 11th International Symposium, Smart Sensor Technology and Measurement Systems*, SanDiego, CA, March 14–18, pp. 148–157.
22. Kirikera, G.R., Shinde, V., Schulz, M.J., Ghoshal, A., Allemang, R. and Sundaresan, M.J. (2006). Damage localization in composite and metallic structures using a structural neural system and simulated acoustic emissions. *Mechanical Systems and Signal Processing*, *21*(*1*), 280–297.
23. Kirikera, G.R., Lee, J.W., Schulz, M.J., Allemang, R., Shanov, V., Ghoshal, A. and Sundaresan, M.J. (2006). Initial evaluation of novel active/passive structural neural system for health monitoring of composite materials. *Journal of Smart Materials and Structures*, *15*(*5*), 1275–1286.
24. Ghoshal, A., Martin, W.N., Schulz, M.J., Chattopadhyay, A. and Prosser, W.H. (2005). Simulation of asymmetric Lamb waves for smart sensing and actuation systems in plates. *Shock and Vibration Journal*, *12*(*4*), 243–271.
25. Kirikera, G.R., Shinde, V., Lee, J.W., Schulz, M.J., Ghoshal, A. and Sundaresan, M.J. (2005). A dual mode active and passive structural neural system for structural health monitoring. *The 5th International Workshop on Structural Health Monitoring*, September 12–14, Stanford, California: Stanford University, pp. 539–546.
26. Lee, J.W., Kirikera, G.R., Kang, I., Schulz, M.J. and Shanov, V. (2006). Structural health monitoring using continuous sensors and neural network analysis. *Smart Materials and Structures*, *15*(*5*), 1266–1274.
27. Patent: Sundaresan, M.J., Ghoshal, A. and Schulz, M.J. (2002). Sensor array system (6,399,939 B1). June.
28. Patent: Sundaresan, M.J., Ghoshal, A. and Schulz, M.J. (2006). System for damage location using a single channel continuous acoustic emission sensor (7,075,424). July 11.
29. Patent Pending: Sundaresan, M.J., Schulz, M.J. and Nkrumah, F. (2006). Systems, methods and computer

program products for characterizing structural events. January.

30. Takemoto, M., Nishino, H. and Ono, K. (2000). Wavelet transform – applications to AE signal analysis. In: Kishi, T., Ohtsu, M. and Yuyama, S. (eds), *Acoustic Emission – Beyond the MILLENNIUM*, Kidlington, Oxford, UK: Elsevier, pp. 35–56.
31. Polikar, R. (2006). The wavelet tutorial. Available at http://users.rowan.edu/~polikar/WAVELETS/WTtutorial.html
32. Wang, L. (2004). Elastic wave propagation in composites and least squares damage localization technique. M.S. Thesis, North Carolina: North Carolina State University.